ChemComm

RSCPublishing

FEATURE ARTICLE

View Article Online
View Journal | View Issue

Observation of growth of metal nanoparticles

Hong-Gang Liao,[a] Kaiyang Niu[a] and Haimei Zheng*[ab]

Cite this: *Chem. Commun.*, 2013, **49**, 11720

Received 30th September 2013,
Accepted 25th October 2013

DOI: 10.1039/c3cc47473a

www.rsc.org/chemcomm

An understanding of nanocrystal growth mechanisms is of significant importance for the design of novel materials. The development of liquid cells for transmission electron microscopy (TEM) has enabled direct observation of nanoparticle growth in a liquid phase. By tracking single particle growth trajectories with high spatial resolution, novel growth mechanisms have been revealed. In recent years, there has been an increasing interest in liquid cell TEM and its applications include real time imaging of nanoparticles, biological materials, liquids, and so on. This paper reviews the development of liquid cell TEM and the progress made in using such a wonderful tool to study the growth of nanoparticles (mostly metal nanoparticles). Achievements in the understanding of coalescence, shape control mechanisms, surfactant effects, *etc.* are highlighted. Other studies relevant to metal precipitation in liquids, such as electrochemical deposition, nanoparticle motion and electron beam effects, are also included. At the end, our perspectives on future challenges and opportunities in liquid cell TEM are provided.

1. Introduction

At the nanoscale, the quantum confinement of a nanocrystal provides the most powerful means to direct the optical, electronic and magnetic properties of the solid material.[1,2] Metal nanocrystals possess many fascinating properties, and they have been applied in a variety of areas including energy technology, life science and environment, such as catalysis,[3] energy conversion and storage,[4,5] electronics,[6,7] information storage,[8] medicine[9,10] and so on. In most of these applications, it requires that nanoparticles are of well controlled size, shape and surface structure.[11,12] For instance, tetrahedral, cubic, and spherical Pt nanocrystals show different activities in the catalytic reactions between hexacyanoferrate(III) and thiosulfate ions.[13] {331} facets exhibit much higher catalytic activities towards oxidation of H_2O_2 than the nanoparticles bound by {111} facets.[14] These examples clearly illustrate the importance of size, shape and structure for efficient utilization of nanoparticles. Most metal nanocrystals share a similar cubic close packed (ccp) structure with a face-centered cubic (fcc) lattice. The properties of a nanoparticle are determined by a set of physical parameters including its composition, size, shape, surface modification, and environment. There has been significant interest in the synthesis of nanocrystals with controlled size, shape and composition.

Synthesis of nanocrystals by colloidal methods has been advanced significantly. Solution based synthesis of nanoparticles with tailored properties has thrived starting from 1990's, although growth of nanoparticles in solution phases can be traced back to 1850's when Michael Faraday prepared his ruby gold by reducing gold chloride with phosphorous in water.[15] In the past two decades, nanocrystals with a variety of shapes including sphere, cube, cuboctahedron, octahedron, tetrahedron, decahedron, icosahedron, thin plate, rod or wire, *etc.* have been achieved. However, the mechanisms of nucleation and growth especially the shape control mechanisms have not been well understood. Thus, practical applications with optimized performance are significantly affected by the poor predictability of the size and morphology of nanoparticles during synthesis. In the absence of a hard template, solution-based methods require precise tuning of the growth conditions to achieve shape control. Factors, such as the reduction potential, temperature, precursor concentration, diffusivity, *etc.* are all important for shape-controlled synthesis.[16] Our understanding of the nucleation and complex growth steps involved in achieving a hierarchical functional structure is limited. The primary barrier for obtaining enough knowledge of nanocrystal formation arises from the difficulty of "seeing through" the liquids to probe chemical and physical events in solvents during nanocrystal growth. This also leads to challenges in understanding the relationship between structure and functionality during material applications.

With the technical advances in electron microscopy and nanofabrication, a new experimental platform, so called liquid cell TEM has emerged, which has made it possible to observe nanocrystal growth in real time. Liquid cell TEM has now been applied to many different nanoparticle systems, where the trajectories of the nanoparticle growth can be obtained. Novel growth mechanisms have been identified although most of

---

[a] *Materials Sciences Division, Lawrence Berkeley National Laboratory, 1 Cyclotron Road, Berkeley, CA 94720, USA. E-mail: hmzheng@lbl.gov*

[b] *Department of Materials Science and Engineering, University of California, Berkeley, CA 94720, USA*

these studies are limited to metal nanoparticle systems. In this review, we show in Section 2.2 the development of liquid cell TEM and discuss the advantages of this technique as compared to other *in situ* methods. In Section 2.3, progress and achievements in the study of metal nanoparticle growth using liquid cell TEM are discussed. Several studies that contributed to the understanding of nanocrystal shape control mechanisms are highlighted. At the end, we provide an outlook of the future opportunities and challenges in the study of nanoparticles or other materials in liquids using liquid cell TEM.

2. Liquid cell TEM study of nanoparticle growth

2.1 The development of liquid cell TEM

The concept of using window confined materials in TEM characterization can be traced back to nearly the beginning of electron microscopy when biological samples were first sandwiched between two thin aluminum foils by Marton in 1934.[17] However, there were limited activities[18–24] in imaging liquid samples using TEM in the next several decades, which is probably because of the incompatibilities of liquids with the high vacuum environment under TEM. Conventional electron microscopes require high vacuum (10^{-6} Torr or higher) within the microscope column, both to allow the operation of the electron source and to minimize scattering other than from the sample. For many decades, the standard characterization protocol for studying kinetics of a reaction process by TEM has been used to image the specimens *ex situ* by stopping the reaction periodically. Unfortunately, many dynamic processes of materials during reactions cannot be obtained using *ex situ* experiments, for example, the growth pathways of many nanocrystals can only be achieved by *in situ* observations.

The recent advances in Micro-Electro-Mechanical Systems (MEMS) have attracted renewed interest and significant progress has been made in liquid environmental TEM. In 2003, Williamson *et al.*[25] reported the development of electrochemical liquid cells for TEM using silicon wafers with the electron transparent silicon nitride membrane window. The gold electrodes were deposited on the patterned bottom chip and it was glued together with the top chip with a glass spacer in between to form an electrochemical liquid cell. Additional containers for liquid electrolyte were assembled in the electrochemical cell for the electric biasing experiments (Fig. 1A). The electrochemical deposition of copper clusters on the gold electrode was studied *in situ*. Since the total thickness of mass that the electron beam penetrating was large (100 nm of each silicon nitride membrane; 50 nm of the gold electrode and liquid thickness over 1 μm), the best resolution of 5 nm was achieved.[26,27] However, in order to study colloidal nanocrystal growth under TEM, a liquid cell needs to offer better resolution. Zheng *et al.* reported a self-contained liquid cell in 2009 and the window membrane thickness was pushed to 25 nm or thinner, which enabled the study of single Pt nanoparticle growth trajectories with sub-nanometer resolution.[28] This work has attracted a lot of attention in the field of colloidal chemistry since it opened the unprecedented opportunity to study nanocrystal growth mechanisms by observation of nanoparticle growth *in situ*. In 2009, de Jonge *et al.*[29] described the use of flow cell to image whole cells in liquids with a constant flow of a buffer solution (Fig. 1C). The liquid flow capability is appealing to researchers who are interested in the study of reactions involving mixing solvents instantaneously or injecting reactant agents. However, critical issues still need to be addressed, such as sample drift introduced by liquid flow, membrane rupture, potential contamination, *etc.*

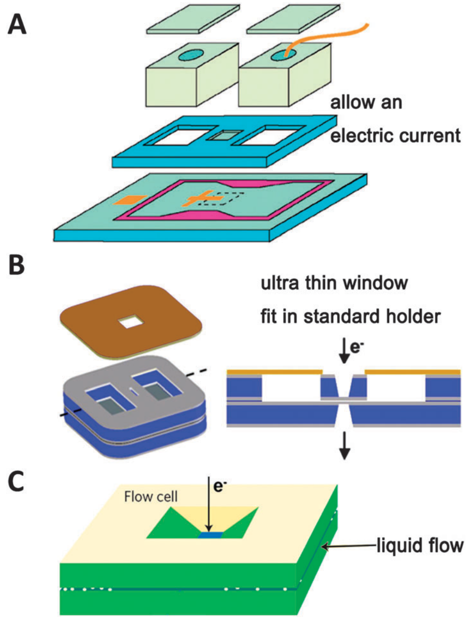

Fig. 1 Schematic of an assembled liquid cell composed of two windows each with the silicon substrate, silicon nitride membrane, and a spacer. (A) Biasing liquid cell.[25] (B) Regular self-contained liquid cell, window: 1 × 50 μm;[28] (C) a microfluidic chamber formed between two microchips in a flow cell.[29]

There has been an increasing interest in liquid cell TEM in recent years. Many other home-made liquid cells have been reported. In general, a windowed environmental liquid cell offers controllable liquid film thickness based upon the spacer height between two thin film membranes, which can be adjusted ranging from tens of nanometers to micrometers. Electrodes with various geometries can be incorporated. Either aqueous or organic solvents can be used in liquid cell experiments to mimic synthetic conditions for nanomaterials. The liquid cell TEM has found a wide range of applications from nanocrystal synthesis to imaging of biological materials, soft materials, the study of electrochemical reactions *in situ*, nanoparticle interaction in liquids and so on. Fig. 2 shows a statistical plot of the published papers using liquid cell methodology over the years and the drastic increase in the number of publications in the last few years is illustrated.[17–74]

2.2 Advantages as compared to other *in situ* methods

For the observation of nanoparticle growth, many methods have been applied, such as the *in situ* optical spectroscopy method,[75] *in situ* X-ray diffraction[76–78] including synchrotron based techniques,[79,80] *in situ* AFM and STM[81–83] and so forth. Oezaslan *et al.*[84] reported the *in situ* measurements of the alloying process of bimetallic Pt–Cu nanoparticles using high-temperature

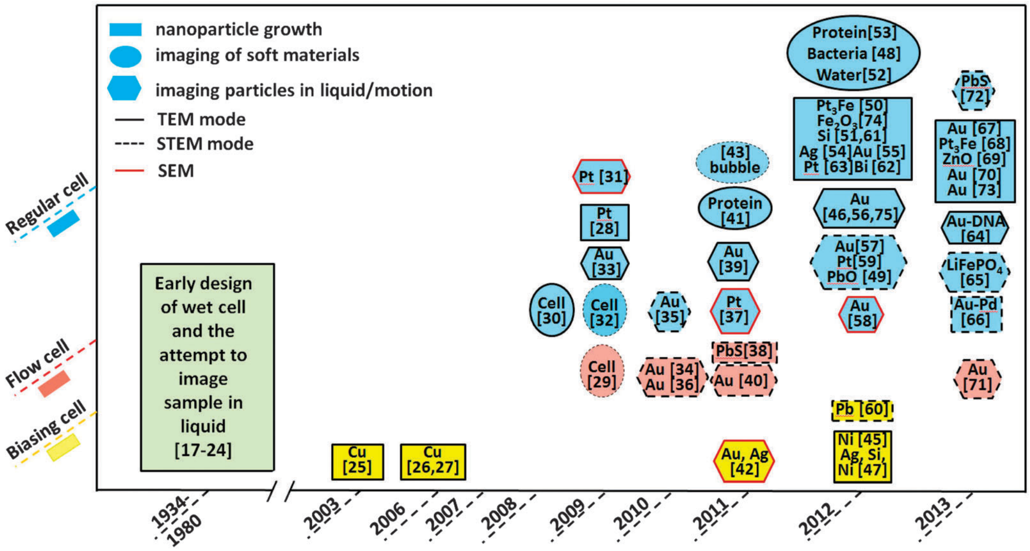

Fig. 2 Publications related to liquid cell electron microscopy since 1934.

X-ray diffraction. Polte *et al.*[77] investigated the growth process of nanoparticles from an average radius of 0.8 nm to about 2 nm by time resolved *in situ* small angle X-ray scattering at millisecond time resolution. Simm *et al.*[82] used *in situ* atomic force microscopy (AFM) to study the growth of cobalt nuclei on a boron doped diamond electrode under potentiostatic control. The rate of growth of the nuclei at the electrode surface is monitored using AFM as a function of time at different deposition potentials. Using these *in situ* methods, critical information on nanoparticle nucleation and growth has been achieved. However, these methods have their limitations, for example, *in situ* spectroscopy methods lack the morphological information; *in situ* AFM and STM can only image samples on a substrate and the temporal resolution is also limited, thus, their applications in colloidal synthesis are restricted.

Compared with other *in situ* methods, liquid cell TEM has its unique advantages that researchers can directly observe the structural and morphological changes of nanoparticles in liquids during the reactions with high spatial resolution. Liquid cell TEM allows atomic resolution imaging to be combined with spectroscopic techniques for chemical identification, such as electron energy loss spectroscopy (EELS), energy dispersive spectroscopy (EDS), *etc.*[49,64,65] The setup is also applicable to a wide range of chemical reactions and soft materials in a liquid phase. It provides a unique platform for the study of nanoparticle formation that alternative analysis methods do not offer. The major criticisms come from the electron beam radiation damage and the challenges in temperature control during reactions. Discussions on these issues will be provided in the later section of this review.

2.3 Progress in metal nanoparticles synthesis by liquid cell TEM

2.3.1 Coalescence *vs.* monomer attachment. Growth through coalescence of nanoparticles (or aggregated growth) has been frequently reported as an alternative to growth by monomer attachment. Nanoparticle coalescence is especially common in metal nanoparticle synthesis and it has been a major concern in size control of nanoparticles. It is generally considered that the coalescence leads to a large nanoparticle size distribution. There have been many studies on the growth kinetics of metal nanoparticles by measuring ensemble particle size distribution at a function of time.[85–90] However, there is no consensus on the role of coalescence during growth. Through real time observation of platinum nanoparticle growth trajectories using liquid cell TEM, Zheng *et al.*[28] compared growth by nanoparticle coalescence with that by monomer attachment side-by-side within the same field of view. It is very interesting that two types of growth reached the same particle size (Fig. 3A). It showed that the coalesced nanoparticle experienced recrystallization and shape re-arrangement, which prevented additional platinum atoms from attaching to the nanoparticle. So, a pause during

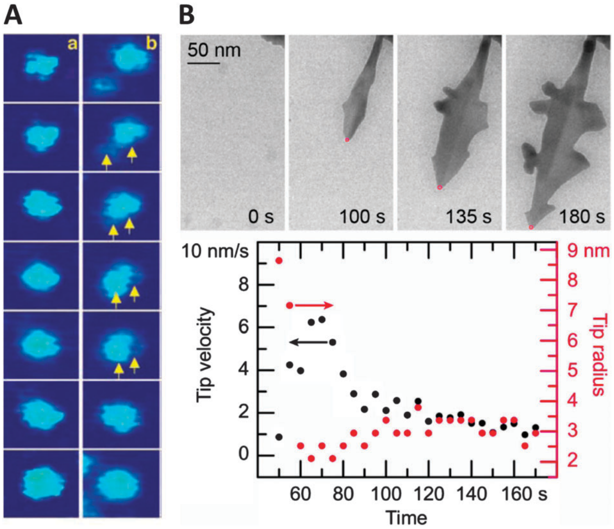

Fig. 3 (A) Video images showing simple growth by monomer addition (left column) or by coalescence (right column).[28] (B) The top row shows growth of the dendrite, the bottom panel shows the velocity and tip radius *versus* time.[66]

growth was observed after a coalescence event, which allowed the nanoparticle by monomer attachment to catch up. Studying single particle growth trajectories makes it possible to obtain such information without ambiguity. Recently, studies by *in situ* X-ray assemble measurements have also confirmed that although there are significant coalescence events during metal nanoparticle growth, monodisperse nanoparticle can be achieved eventually.[76,91]

It has been reported that coalescence as an alternative to simple growth by attachment of monomeric species plays an important role in the synthesis of many other nanocrystals with more complex shapes.[67,89,92–94] However, there is no doubt that conventional growth by monomer attachment is still commonly observed. Tracking the growth of nanostructures *in situ*, such as dendritic growth of gold, was reported by Kraus *et al.*[66] (Fig. 3B). Dendrite nucleation was induced by the electron beam which led to an initial burst of growth. During the subsequent growth process gold nanoparticles were covered with a thin liquid layer of precursor solution. The tip growth velocity between 0.1 and 2.0 nm s^{-1} was observed. Tip velocity fluctuations were captured among different dendrite geometries grown from the tips. Those dendrites showing granularities in their structure experienced the largest growth speed. By comparison of the observed velocities with diffusion-limited growth rates, they concluded that the dendrite growth at this scale was limited by diffusion.

2.3.2 Shape control mechanisms and surfactant effects. Synthesis of nanocrystals with different shape and architecture has been a topic of significant interest.[95–100] Many factors, such as precursor concentration, temperature, surfactants, *etc.* can alter the chemical potential of crystallization in liquids, thus the shape of the nanocrystals differs under different growth conditions.[95,101–103]

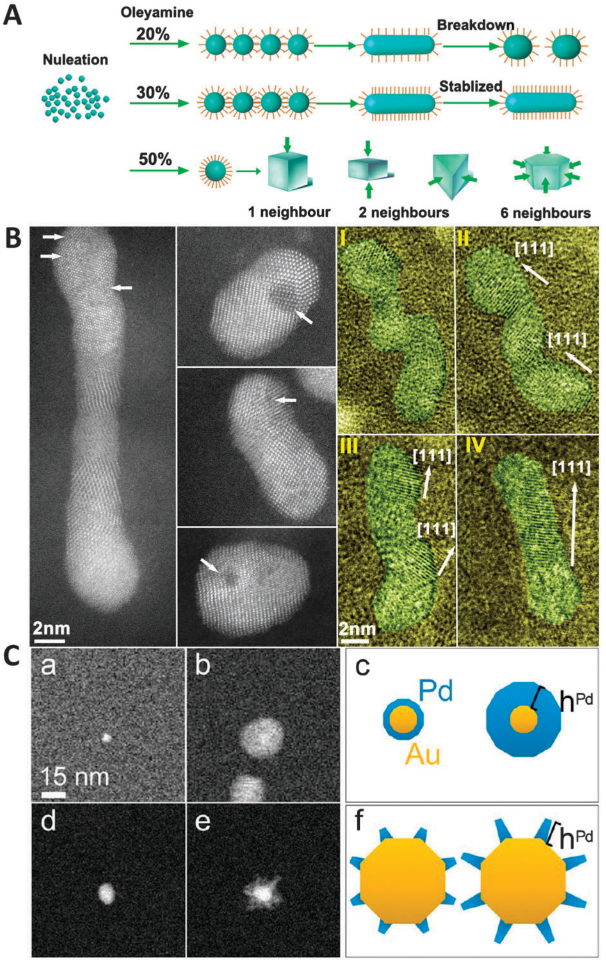

Fig. 4 (A) Schematic showing the surfactant (oleylamine) effect and stereo-hindrance effects during growth. High-resolution STEM images of Pt_3Fe nanorods and the dynamic shape and orientation changes during structural relaxation. (B) HAADF STEM image of a polycrystalline Pt_3Fe nanorod, dimers, and nanoparticles obtained in a liquid cell. The dark spots (highlighted by arrows) indicate the iron-rich regions (left). Sequential HRTEM images (I to IV) show both crystal orientation and shape changes during the straightening of a twisted nanoparticle chain (right). (C) Comparison of Pd growth on 5 and 15 nm Au seeds. (a–d) Dark-field STEM images of the two sized nanoparticles grown in a 10 μM aqueous $PdCl_2$ solution. (b, e) The same two particles after Pd deposition. (c, f) Schematic illustration of the Pd morphologies grown from two different sized Au seeds. Note: images are from the original publications.[49,50,67]

Using Pt–Fe nanocrystals as a model system, Liao *et al.* systematically studied the effects of oleylamine concentration on the shape evolution of platinum iron nanocrystals[67] (Fig. 4A). A self-contained liquid cell with ultra thin silicon nitride membranes was used. Superb spatial resolution with atomic level elemental information through high angle annular dark field (HAADF) scanning TEM (STEM) was achieved although they appear to be *ex situ* snap shot images[50] (Fig. 4B). The direct observation revealed that with a relatively low concentration of oleylamine (20%), there were three stages of growth: (I) nucleation and growth of platinum iron nanoparticles in the precursor solution; (II) end-to-end nanoparticle attachment to form nanowires; (III) breakdown or shrinkage of the nanowires into individual nanoparticles with large size distribution. With 30% oleylamine, platinum iron nanowires were obtained through shape directed nanoparticle attachment, which was similar to that with 20% oleylamine. However, nanowires were stabilized in the growth solution with 30% oleylamine and they did not break down or shrink. As the concentration of oleylamine increased to 50%, individual nanoparticles were stable in solution and merging between nanoparticles at the later stage was avoided. Visualization of Pt–Fe nanorod growth in 30% oleylamine clearly showed that nanoparticles preferred to attach in one dimension, which suggests the prominence of dipolar interactions between nanoparticles. Such interactions were quantified for the first time by measuring motions of nanocrystals and rearrangement of the nanocrystal grains to accommodate the lattice mismatch of the nanocrystals.

Their studies also demonstrated that shape evolution of a nanocrystal was strongly influenced by neighboring particles due to the stereo hindrance effect, and the oleylamine (surfactant) effect on shape evolution of a nanoparticle was secondary to the effects of neighboring nanoparticles.

Jungjohann *et al.*[49] investigated Pd growth in a dilute aqueous Pd salt solutions containing Au nanoparticle seeds (Fig. 4C). Au–Pd core–shell nanostructures were formed *via* deposition of Pd^0, generated by the reduction of chloropalladate complexes by radicals, such as hydrated electrons in the solution induced by electron beam. They showed that size and shape of the Au seeds determine the morphology of the Pd shells, *via* preferential Pd incorporation in low-coordination sites and avoidance of extended facets. Analysis of the Pd incorporation on Au particles at different distances from a focused electron beam provided a quantitative picture of the growth process. The growth was limited by the ion diffusion in the solution.

2.3.3 High resolution imaging using graphene liquid cells. Recently, graphene liquid cells have been emerged (Fig. 5A), which use two layers of graphene to trap thin liquids for *in situ* TEM. The graphene liquid cell has enabled the study of colloidal nanocrystal growth with excellent high resolution imaging (Fig. 4B). This is because electron scattering due to the membrane window can be minimized. Yuk *et al.*[62] used this new type of liquid cell to explore the mechanism of platinum nanocrystal growth and discovered site-selective coalescence, structural reshaping after coalescence, and surface faceting along the growth trajectories. Recently, graphene liquid cells have also been applied to the study of 3D motion of DNA linked gold nanoparticles in liquids[63] (Fig. 5C). Although only pockets of liquids can be trapped in such graphene liquid cells, the high resolution imaging and the ease of fabrication open many opportunities for future studies of nanoparticle growth or other systems.

2.3.4 Electrochemical liquid cells and electrodeposition. The electrochemical deposition of metal clusters or dendritic structures[25,47] has attracted a lot of attention due to its relevance to batteries or other energy storage devices. Using an electrochemical cell similar to the earlier work, White *et al.*[59] reported the electrochemical deposition of lead from an aqueous solution of lead(II) nitrate. Both the lead deposits and the local Pb^{2+} concentration were visualized. Depending on the rate of potential change and the potential history, lead deposited on the cathode was either a compact layer or dendrites. In both cases the deposits were removed when the electric bias was reversed. Asperities that persist through many plating and stripping cycles consistently nucleated larger dendrites. Quantitative image analysis showed an excellent correlation between changes in the Pb^{2+} concentration or the rate of lead deposition and the current passed through the electrochemical cell. These real-time observations of nanomaterial growth and transformations using liquid cell TEM provided a lot of critical information on the electrochemical processes important for the development of energy storage technologies.

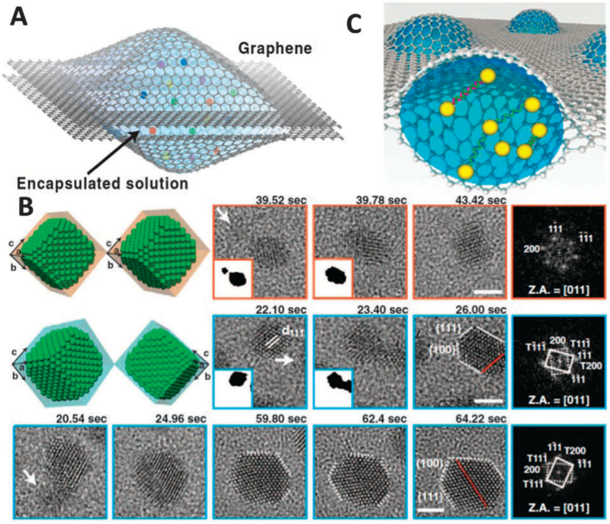

Fig. 5 (A) Illustration of graphene liquid cell (GLC) encapsulating the growth solution. (B) Still snapshots of Pt nanocrystal growth *via* coalescence and crystal-structure evolution observed with atomic resolution in a GLC. (C) Illustration of DNA–Au nanoconjugates in a graphene cell. All images can be found in the original publication.[62]

2.3.5 Nanoparticle motion. During nanoparticle synthesis, nanoparticles may move around rigorously in solution. Motion of nanoparticles in the growth solution may come from Brownian motion, chemical reaction induced local environment changes, liquid flow, electron beam effects, *etc.* An understanding of the physics and the origin of nanoparticle motion is important for many other studies using liquid cell TEM.

So far, there have been many reports on nanoparticle motion imaged by liquid cell TEM. Both self-contained liquid cells[33] and flow cells[36,46] have been used. Zheng *et al.*[33] studied the diffusion of spherical and rod-shape gold nanoparticles in water with 15% glycerol. It was observed that nanoparticles show random Brownian motion plus jumps. Long distance motion due to liquid drag was also recorded. de Jonge *et al.*[34] used STEM to image gold nanoparticles in several micrometers thickness water. White *et al.*[58] studied the charged Pt nanoparticle dynamics in water. Mueller *et al.*[70] captured motion of gold nanorods in a flow cell. Liu *et al.*[69] studied the self-assembly of charged gold nanoparticles in liquid. Park *et al.*[55] directly observed nanoparticle super lattice formation. There are other reports on imaging nanoparticle motion, but only to prove their liquid cell device is functional under TEM.

2.3.6 Reduction mechanisms and electron beam effects. Most studies on nanoparticle synthesis by liquid cell TEM use electron beam as the reducing agent to reduce metal precursors in the growth solution. As to an electrochemical deposition, the electric potential is the driving force for metal structure growth, which often introduces large clusters or dendritic structures.[25,47] Xin *et al.*[61] reported the first observation of oscillatory growth of Bi at an elevated temperature of 180 °C using liquid cell TEM (Fig. 6B). An electron beam has perceptible effects on the liquid solution. Besides the reduction of the metal precursor, it can produce bubbles in liquids, generate solvated ions or electrons and rupture the liquid film.[58,72] Thus, the reactions under electron beam irradiation can be complex. Although electron beam effects are pronounced in many reports, the study of nanoparticle growth using liquid cell TEM is of great interest to many researchers. It is well known that the synthetic approach to colloidal nanocrystals is extremely diverse. Besides the common thermal heating, growth can be initiated by an electrochemical potential,[99] microwave,[104,105] solar light,[106] biomineralization,[88,107,108] electron beam irradiation[109,110] and so forth. Electron beam induced nanoparticle growth using liquid cell TEM falls into the above wide spectra of growth. Efforts to elucidate nanoparticle growth mechanisms under electron beam irradiation are highly valuable for the understanding of nanocrystal growth in general.

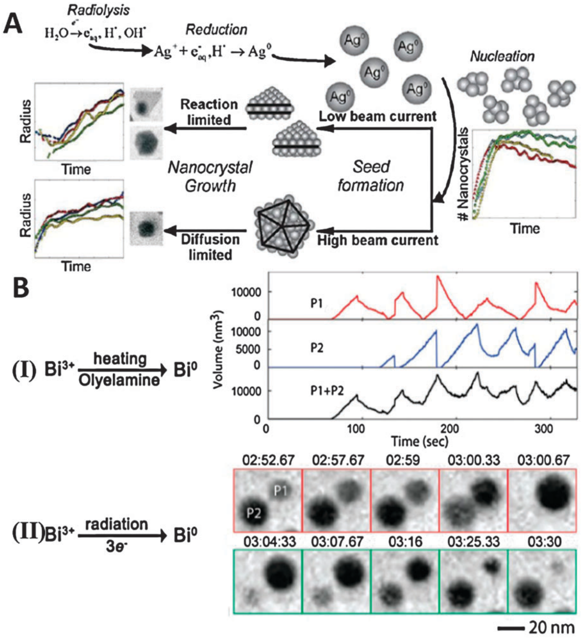

Fig. 6 (A) Schematic of beam induced growth of Ag nanoparticles.[60] (B) Oscillatory growth of Bi nanoparticles; top: the total volume of the ensemble and a few selected particles *vs.* time, bottom: trajectories of two particles (P1 and P2) showing pairwise oscillation.[61]

Woehl *et al.*[60] studied silver particle growth by using a flow cell and found that electron beam current played a major role in controlling the morphology of silver nanocrystals (Fig. 6A). It was demonstrated that under a low beam current reaction limited growth was preferred and nanocrystals with faceted structures were achieved. Under a higher beam current, diffusion limited growth was dominant and nanocrystals with more complex shape were achieved. Isolation of these two growth regimes showed a new level of control over nanocrystal growth under electron beam irradiation. In the future, more quantitative study of reaction mechanisms will certainly be highly beneficial to the understanding of electron induced growth and to the growth of *in situ* electron microscopy field in general.

3. Conclusion and outlook

In situ liquid cell TEM is one of the recent advances in characterization of solution-phase reactions. It allows us to track morphological, structural and chemical changes of solids in liquids in real time. Nucleation and growth of nanoparticles occur dynamically and they are surrounded by solvent and other molecules, which present challenges to *in situ* measurements. Hence, there are only a few techniques that can address issues on the mechanisms of nanoparticle growth through *in situ* studies. *In situ* liquid cell TEM with a combination of temporal and spatial resolution shows many advantages over many other characterization techniques. This has enabled the understanding of nanocrystal growth with an unprecedented level of information. The growing interest in liquid cell TEM has been demonstrated by the drastic increase of the number of publications. This review has provided an overview of this exciting technique and its applications in real-time observation of colloidal nanoparticle growth.

Real time observation of the dynamic growth process sheds light on the nanocrystal growth mechanisms, and points the way towards the synthesis of nanomaterials with desired properties. However, due to the short time of development of the modern liquid cell TEM, many important issues still need to be addressed. For example, nanoparticles in fluids normally move, which can lead to them becoming out of focus, thus affecting the imaging quality especially at higher magnification or at an elevated temperature. Liquids with high vapour pressure including pure water are hard to handle since they can easily dry out at sample loading or vanish under electron beam irradiation, which increases the experimental challenge and limits the application of liquid cell TEM techniques. Most colloidal synthesis proceeds by hot injection (mixing precursor solution together at a certain temperature for reactions), reactions by solvent mixing have not been achieved by the current liquid cell setup. Although ultra-thin silicon nitride membranes and graphene have been incorporated in the new liquid cell design, resolution still needs to be improved in many cases where electron beam scattering is largely from a thick liquid layer, therefore controlled thinning of liquid layer thickness is required. Other future developments include low dose imaging to reduce electron beam damage, faster imaging to capture fast reaction dynamics, weak contrast imaging to enhance the contrast of soft materials, *etc.* The ultimate goal of liquid cell TEM is to resolve single molecule interactions during a liquid phase reaction. In order to reach such a level, there is still large room for development. There is no doubt that the liquid cell TEM technique will play an increasingly important role in discovering nanocrystal growth mechanisms and a wide range of other material transformations in materials science, chemistry and biological science.

Acknowledgements

We thank the funding support of DOE Office of Science Early Career Research Program.

Notes and references

1 Y. Xia, Y. Xiong, B. Lim and S. E. Skrabalak, *Angew. Chem., Int. Ed.*, 2009, **48**, 60–103.
2 Y. N. Xia, B. Gates, Y. D. Yin and Y. Lu, *Adv. Mater.*, 2000, **12**, 693–713.
3 S. H. Joo, S. J. Choi, I. Oh, J. Kwak, Z. Liu, O. Terasaki and R. Ryoo, *Nature*, 2001, **412**, 169–172.
4 W. U. Huynh, J. J. Dittmer and A. P. Alivisatos, *Science*, 2002, **295**, 2425–2427.
5 I. Gur, N. A. Fromer, M. L. Geier and A. P. Alivisatos, *Science*, 2005, **310**, 462–465.
6 A. G. Dong, J. Chen, P. M. Vora, J. M. Kikkawa and C. B. Murray, *Nature*, 2010, **466**, 474–477.
7 S. Jeong, K. Woo, D. Kim, S. Lim, J. S. Kim, H. Shin, Y. Xia and J. Moon, *Adv. Funct. Mater.*, 2008, **18**, 679–686.
8 C. B. Murray, S. H. Sun, H. Doyle and T. Betley, *MRS Bull.*, 2001, **26**, 985–991.
9 A. K. Gupta and M. Gupta, *Biomaterials*, 2005, **26**, 3995–4021.
10 J. Panyam and V. Labhasetwar, *Adv. Drug Delivery Rev.*, 2003, **55**, 329–347.
11 A. R. Tao, S. Habas and P. Yang, *Small*, 2008, **4**, 310–325.

12 M. C. Daniel and D. Astruc, *Chem. Rev.*, 2004, **104**, 293–346.
13 R. Narayanan and M. A. El-Sayed, *Nano Lett.*, 2004, **4**, 1343–1348.
14 H. G. Liao, Y. X. Jiang, Z. Y. Zhou, S. P. Chen and S. G. Sun, *Angew. Chem., Int. Ed.*, 2008, **47**, 9100–9103.
15 M. Faraday, *Philos. Trans. R. Soc. London*, 1857, **147**, 145–181.
16 V. N. Richards, N. P. Rath and W. E. Buhro, *Chem. Mater.*, 2010, **22**, 3556–3567.
17 L. Marton, *Acad. R. Belg., Bull. Cl. Sci.*, 1934, **20–133**, 439–911.
18 I. M. Abrams and J. W. McBain, *J. Appl. Phys.*, 1944, **15**, 607–609.
19 J. A. Swift and A. C. Brown, *J. Phys. E: Sci. Instrum.*, 1970, **3**, 924–926.
20 E. P. Butler, *Rep. Prog. Phys.*, 1979, **42**, 833–889.
21 E. F. Fullam, *Rev. Sci. Instrum.*, 1972, **43**, 245–247.
22 G. Dupouy, F. Perrier and L. Durrieu, *C. R. Hebd. Seances Acad. Sci.*, 1962, **254**, 3786–3791.
23 D. L. Allinson, *Proceedings of the 7th international congress on electron microscopy*, 1970, 169–170.
24 A. Fukami, T. Etoh, N. Ishihara, M. Katoh and K. Fujiwara, *Proceedings of the 7th international congress on electron microscopy*, 1970, 171–172.
25 M. J. Williamson, R. M. Tromp, P. M. Vereecken, R. Hull and F. M. Ross, *Nat. Mater.*, 2003, **2**, 532–536.
26 A. Radisic, F. Ross and P. Searson, *J. Phys. Chem. B*, 2006, **110**, 7862–7868.
27 A. Radisic, P. M. Vereecken, J. B. Hannon, P. C. Searson and F. M. Ross, *Nano Lett.*, 2006, **6**, 238–242.
28 H. Zheng, R. K. Smith, Y.-w. Jun, C. Kisielowski, U. Dahmen and A. P. Alivisatos, *Science*, 2009, **324**, 1309–1312.
29 N. de Jonge, D. B. Peckys, G. J. Kremers and D. W. Piston, *Proc. Natl. Acad. Sci. U. S. A.*, 2009, **106**, 2159–2164.
30 K.-L. Liu, C.-C. Wu, Y.-J. Huang, H.-L. Peng, H.-Y. Chang, P. Chang, L. Hsu and T.-R. Yew, *Lab Chip*, 2008, **8**, 1915–1921.
31 E. U. Donev and J. T. Hastings, *Nano Lett.*, 2009, **9**, 2715–2718.
32 D. B. Peckys, G. M. Veith, D. C. Joy and N. de Jonge, *PLoS One*, 2009, **4**, e8214.
33 H. M. Zheng, S. A. Claridge, A. M. Minor, A. P. Alivisatos and U. Dahmen, *Nano Lett.*, 2009, **9**, 2460–2465.
34 N. de Jonge, N. Poirier-Demers, H. Demers, D. B. Peckys and D. Drouin, *Ultramicroscopy*, 2010, **110**, 1114–1119.
35 J. M. Grogan and H. H. Bau, *J. Microelectromech. Syst.*, 2010, **19**, 885–894.
36 E. A. Ring and N. de Jonge, *Microsc. Microanal.*, 2010, **16**, 622–629.
37 E. U. Donev, G. Schardein, J. C. Wright and J. T. Hastings, *Nanoscale*, 2011, **3**, 2709–2717.
38 J. E. Evans, K. L. Jungjohann, N. D. Browning and I. Arslan, *Nano Lett.*, 2011, **11**, 2809–2813.
39 J. M. Grogan, L. Rotkina and H. H. Bau, *Phys. Rev. E: Stat., Nonlinear, Soft Matter Phys.*, 2011, **83**, 061405.
40 K. L. Klein, I. M. Anderson and N. De Jonge, *J. Microsc.*, 2011, **242**, 117–123.
41 D. B. Peckys, M. J. Dukes, E. A. Ring, D. W. Piston and N. de Jonge, *Microsc. Today*, 2011, **19**, 16–20.
42 M. Suga, H. Nishiyama, Y. Konyuba, S. Iwamatsu, Y. Watanabe, C. Yoshiura, T. Ueda and C. Sato, *Ultramicroscopy*, 2011, **111**, 1650–1658.
43 E. R. White, M. Mecklenburg, S. B. Singer, S. Aloni and B. C. Regan, *Appl. Phys. Express*, 2011, **4**, 055201.
44 N. D. Browning, M. A. Bonds, G. H. Campbell, J. E. Evans, T. LaGrange, K. L. Jungjohann, D. J. Masiel, J. McKeown, S. Mehraeen, B. W. Reed and M. Santala, *Curr. Opin. Solid State Mater. Sci.*, 2012, **16**, 23–30.
45 X. Chen, K. W. Noh, J. G. Wen and S. J. Dillon, *Acta Mater.*, 2012, **60**, 192–198.
46 X. Chen and J. Wen, *Nanoscale Res. Lett.*, 2012, **7**, 1–6.
47 X. Chen, L. H. Zhou, P. Wang, C. J. Zhao and X. L. Miao, *Chin. J. Chem.*, 2012, **30**, 2839–2843.
48 T.-W. Huang, S.-Y. Liu, Y.-J. Chuang, H.-Y. Hsieh, C.-Y. Tsai, Y.-T. Huang, U. Mirsaidov, P. Matsudaira, F.-G. Tseng, C.-S. Chang and F.-R. Chen, *Lab Chip*, 2012, **12**, 340–347.
49 K. L. Jungjohann, J. E. Evans, J. A. Aguiar, I. Arslan and N. D. Browning, *Microsc. Microanal.*, 2012, **18**, 621–627.
50 H.-G. Liao, L. Cui, S. Whitelam and H. Zheng, *Science*, 2012, **336**, 1011–1014.
51 U. M. Mirsaidov, H. Zheng, D. Bhattacharya, Y. Casana and P. Matsudaira, *Proc. Natl. Acad. Sci. U. S. A.*, 2012, **109**, 7187–7190.
52 U. M. Mirsaidov, H. Zheng, Y. Casana and P. Matsudaira, *Biophys. J.*, 2012, **102**, L15–L17.
53 Y. Liu, X. Chen, K. W. Noh and S. J. Dillon, *Nanotechnology*, 2012, **23**, 385302.
54 J. Park, S. Kodambaka, F. M. Ross, J. M. Grogan and H. H. Bau, *Microsc. Microanal.*, 2012, **18**, 1098–1099.
55 J. Park, H. M. Zheng, W. C. Lee, P. L. Geissler, E. Rabani and A. P. Alivisatos, *ACS Nano*, 2012, **6**, 2078–2085.
56 E. A. Ring and N. de Jonge, *Micron*, 2012, **43**, 1078–1084.
57 J. D. Stoll and A. Kolmakov, *Nanotechnology*, 2012, **23**, 505704.
58 E. R. White, M. Mecklenburg, B. Shevitski, S. B. Singer and B. C. Regan, *Langmuir*, 2012, **28**, 3695–3698.
59 E. R. White, S. B. Singer, V. Augustyn, W. A. Hubbard, M. Mecklenburg, B. Dunn and B. C. Regan, *ACS Nano*, 2012, **6**, 6308–6317.
60 T. J. Woehl, J. E. Evans, I. Arslan, W. D. Ristenpart and N. D. Browning, *ACS Nano*, 2012, **6**, 8599–8610.
61 H. L. Xin and H. Zheng, *Nano Lett.*, 2012, **12**, 1470–1474.
62 J. M. Yuk, J. Park, P. Ercius, K. Kim, D. J. Hellebusch, M. F. Crommie, J. Y. Lee, A. Zettl and A. P. Alivisatos, *Science*, 2012, **336**, 61–64.
63 A. P. Alivisatos, Q. Chen, J. Smith, J. Park, K. Kim, D. Ho, H. I. Rasool and A. Zettl, *Nano Lett.*, 2013, **13**, 4556–4561.
64 M. E. Holtz, Y. C. Yu, J. Gao, H. D. Abruna and D. A. Muller, *Microsc. Microanal.*, 2013, **19**, 1027–1035.
65 K. L. Jungjohann, S. Bliznakov, P. W. Sutter, E. A. Stach and E. A. Sutter, *Nano Lett.*, 2013, **13**, 2964–2970.
66 T. Kraus and N. de Jonge, *Langmuir*, 2013, **29**, 8427–8432.
67 H. G. Liao and H. M. Zheng, *J. Am. Chem. Soc.*, 2013, **135**, 5038–5043.
68 Y. Liu, K. Tai and S. J. Dillon, *Chem. Mater.*, 2013, **25**, 2927–2933.
69 Y. Z. Liu, X. M. Lin, Y. G. Sun and T. Rajh, *J. Am. Chem. Soc.*, 2013, **135**, 3764–3767.
70 C. Mueller, M. Harb, J. R. Dwyer and R. D. Miller, *J. Phys. Chem. Lett.*, 2013, **4**, 2339–2347.
71 D. A. Welch, R. Faller, J. E. Evans and N. D. Browning, *Ultramicroscopy*, 2013, **135**, 36–42.
72 T. J. Woehl, K. L. Jungjohann, J. E. Evans, I. Arslan, W. D. Ristenpart and N. D. Browning, *Ultramicroscopy*, 2013, **127**, 53–63.
73 D. S. Li, M. H. Nielsen, J. R. I. Lee, C. Frandsen, J. F. Banfield and J. J. De Yoreo, *Science*, 2012, **336**, 1014–1018.
74 H. Zheng, U. M. Mirsaidov, L.-W. Wang and P. Matsudaira, *Nano Lett.*, 2012, **12**, 5644–5648.
75 J. Becker, O. Schubert and C. Sonnichsen, *Nano Lett.*, 2007, **7**, 1664–1669.
76 B. Abecassis, F. Testard, O. Spalla and P. Barboux, *Nano Lett.*, 2007, **7**, 1723–1727.
77 J. Polte, R. Erler, A. F. Thuenemann, S. Sokolov, T. T. Ahner, K. Rademann, F. Emmerling and R. Kraehnert, *ACS Nano*, 2010, **4**, 1076–1082.
78 N. Steinfeldt, *Langmuir*, 2012, **28**, 13072–13079.
79 J. Miao, C.-C. Chen, C. Song, Y. Nishino, Y. Kohmura, T. Ishikawa, D. Ramunno-Johnson, T.-K. Lee and S. H. Risbud, *Phys. Rev. Lett.*, 2006, **97**, 215503.
80 Y. Sun and Y. Ren, *Part. Part. Syst. Charact.*, 2013, **30**, 399–419.
81 G. V. Ramesh, B. Sreedhar and T. P. Radhakrishnan, *Phys. Chem. Chem. Phys.*, 2009, **11**, 10059–10063.
82 A. O. Simm, X. B. Ji, C. E. Banks, M. E. Hyde and R. G. Compton, *ChemPhysChem*, 2006, **7**, 704–709.
83 A. Kolmakov and D. W. Goodman, *Chem. Rec.*, 2002, **2**, 446–457.
84 M. Oezaslan, F. Hasche and P. Strasser, *Chem. Mater.*, 2011, **23**, 2159–2165.
85 S. P. Shields, V. N. Richards and W. E. Buhro, *Chem. Mater.*, 2010, **22**, 3212–3225.
86 F. Wang, A. Dong, J. Sun, R. Tang, H. Yu and W. E. Buhro, *Inorg. Chem.*, 2006, **45**, 7511–7521.
87 R. L. Penn and J. F. Banfield, *Science*, 1998, **281**, 969–971.
88 J. F. Banfield, S. A. Welch, H. Z. Zhang, T. T. Ebert and R. L. Penn, *Science*, 2000, **289**, 751–754.
89 Y. Yin and A. P. Alivisatos, *Nature*, 2005, **437**, 664–670.
90 Z. Y. Tang and N. A. Kotov, *Adv. Mater.*, 2005, **17**, 951–962.
91 G. Renaud, R. Lazzari, C. Revenant, A. Barbier, M. Noblet, O. Ulrich, F. Leroy, J. Jupille, Y. Borensztein, C. R. Henry, J. P. Deville, F. Scheurer, J. Mane-Mane and O. Fruchart, *Science*, 2003, **300**, 1416–1419.
92 R. L. Penn and J. F. Banfield, *Geochim. Cosmochim. Acta*, 1999, **63**, 1549–1557.

93 K. S. Cho, D. V. Talapin, W. Gaschler and C. B. Murray, *J. Am. Chem. Soc.*, 2005, **127**, 7140–7147.

94 N. Gehrke, H. Colfen, N. Pinna, M. Antonietti and N. Nassif, *Cryst. Growth Des.*, 2005, **5**, 1317–1319.

95 X. G. Peng, L. Manna, W. D. Yang, J. Wickham, E. Scher, A. Kadavanich and A. P. Alivisatos, *Nature*, 2000, **404**, 59–61.

96 Y. G. Sun and Y. N. Xia, *Science*, 2002, **298**, 2176–2179.

97 C. Pacholski, A. Kornowski and H. Weller, *Angew. Chem., Int. Ed.*, 2002, **41**, 1188–1191.

98 D. J. Milliron, S. M. Hughes, Y. Cui, L. Manna, J. B. Li, L. W. Wang and A. P. Alivisatos, *Nature*, 2004, **430**, 190–195.

99 N. Tian, Z.-Y. Zhou, S.-G. Sun, Y. Ding and Z. L. Wang, *Science*, 2007, **316**, 732–735.

100 B. Lim, M. Jiang, P. H. C. Camargo, E. C. Cho, J. Tao, X. Lu, Y. Zhu and Y. Xia, *Science*, 2009, **324**, 1302–1305.

101 D. V. Leff, L. Brandt and J. R. Heath, *Langmuir*, 1996, **12**, 4723–4730.

102 B. Nikoobakht and M. A. El-Sayed, *Chem. Mater.*, 2003, **15**, 1957–1962.

103 G. Xiang, J. Zhuang and X. Wang, *Inorg. Chem.*, 2009, **48**, 10222–10230.

104 X. H. Liao, N. Y. Chen, S. Xu, S. B. Yang and J. J. Zhu, *J. Cryst. Growth*, 2003, **252**, 593–598.

105 A. B. Panda, G. Glaspell and M. S. El-Shall, *J. Am. Chem. Soc.*, 2006, **128**, 2790–2791.

106 O. Akhavan and E. Ghaderi, *J. Phys. Chem. C*, 2009, **113**, 20214–20220.

107 A. P. Alivisatos, *Science*, 2000, **289**, 736–737.

108 H. Colfen and S. Mann, *Angew. Chem., Int. Ed.*, 2003, **42**, 2350–2365.

109 Z. Li, Z. Jiao, M. Wu, Q. Liu, H. Zhong and X. Geng, *Colloids Surf., A*, 2008, **313**, 40–42.

110 Z. Li, L. Peng, Y. Fang, Z. Chen, D. Pan and M. Wu, *Radiat. Phys. Chem.*, 2011, **80**, 1333–1336.